Runoff and infiltration estimates based on pore pressure changes in shallow aquitards

Amirhossein Shafaei, François Duhaime & Michel Baraër
École de technologie supérieure (ÉTS), Montreal, Quebec, Canada
Vahid Marefat
BBA, Montreal, Quebec, Canada

ABSTRACT
The pore pressure time series that are recorded by piezometers installed in clay aquitards can be used to study the local water budget. For deep aquitards, pore pressure time series corrected for barometric pressure changes and earth tides can be related to the moisture loading at the top of the soil profile. When compared with precipitation and evapotranspiration, the moisture loading allows runoff and infiltration to be calculated. For shallow aquitards, the pore pressure record can be more complex as pore pressure changes due to seasonal fluctuations of the water table are superimposed on the total stress changes due to moisture loading. In this study, a finite element model was developed with COMSOL Multiphysics and its MATLAB LiveLink interface to calculate the moisture loading from complex pore pressure record in shallow aquitards. The MATLAB script discretizes the simulation in a series of time steps. The script iterates on the total stress boundary condition for each time step to replicate the pore pressure measured in the field. The paper presents a case study for the Sainte-Marthe test site in near Montreal, Canada.

RÉSUMÉ
Les séries temporelles de pression interstitielle enregistrées par les piézomètres installés dans les couches d'argile permettent d'étudier le bilan hydrique local. Pour les aquitards profonds, les séries temporelles de pression interstitielle corrigées pour les variations de la pression atmosphérique et les marées terrestres peuvent être utilisées pour évaluer les variations de contraintes associées à l'humidité qui est stockée au sommet du profil de sol. Avec les précipitations et l'évapotranspiration, ces variations peuvent être utilisées pour calculer le ruissellement et l'infiltration. Pour les aquitards peu profonds, les séries temporelles de pression interstitielle peuvent être plus complexes en raison des fluctuations saisonnières de la nappe phréatique qui se superposent aux variations de la contrainte totale dues à la charge en humidité. Dans ce projet, un modèle d'éléments finis a été développé avec COMSOL Multiphysics et son interface MATLAB LiveLink pour calculer la charge en humidité pour les aquitards peu profonds à partir de séries temporelles de pression interstitielle complexes. Le script MATLAB discrétise la simulation en une série de pas de temps. Le script itère sur la condition à la frontière sur la contrainte totale pour chaque pas de temps afin de reproduire la pression interstitielle mesurée sur le terrain. L'article présente un exemple pour le site expérimental de Sainte-Marthe, près de Montréal, Canada.

1. INTRODUCTION

Micro-scale studies of soil behaviour show that soil stability is the result of a balance between various internal forces. A change in any of these forces will lead to alteration of other forces for compensation and to maintain balance. For instance, a change in the total vertical stress will be followed by a change in pore pressure and effective stress resulting in a high correlation between mechanical loads on the ground surface and hydraulic head fluctuations in confined aquifers or aquitards.

Hydraulic head or pore pressure time series can be used to analyze the soil water balance (van der Kamp and Schmidt 2017). The idea of using pore pressure records for estimating the water budget in the soil profile comes from an approach proposed by van der Kamp and Gale (1983) which itself was derived from the Biot (1941) theory by considering some simplifications and assumptions. Based on this approach, if the tidal and barometric effects are subtracted from the observed hydraulic heads, the remaining fluctuations are strongly correlated to the changes in soil moisture loading induced by precipitations, runoff and evapotranspiration (van der Kamp and Maathuis 1991). The ideal situation for implanting this approach is within thick aquitards or within aquifers fully confined by thick aquitards where the impact of transient flow on hydraulic head changes in the soil is minimum. The low permeability of aquitards isolates them from the pore pressure changes at their top and bottom boundaries (Barr et al. 2000).

Pore pressure changes in thick aquitards are most likely to reflect only the mechanical loading on the formation (van der Kamp and Schmidt 2017). Anochikwa et al. (2012) considered this characteristic of aquitards and simulated the pore pressure variation induced by surface loading and groundwater level fluctuations utilizing a coupled stress-flow code. Based on a superposition technique, they applied a new approach based on the van der Kamp and Gale (1983) theory to replicate separately the pore pressure response to mechanical loading or water table fluctuations in a stiff clay layer below a surficial layer of gravel and sand. Their study also showed that by increasing the aquitard thickness, the impact of water-table transients is less significant and hydraulic head changes within the aquitard reflect more accurately the mechanical loading induced by soil moisture fluctuations. Other studies have analyzed the pore pressure variations in soil and rock for the assessment of soil moisture balance (e.g., Marin et

al. 2010; Hayashi and Farrow 2014; Smith et al. 2017).

Other applications based on the interpretation of pore pressure time series have been developed. For instance, Chen et al. (2015) applied this method to investigate the relationship between groundwater level fluctuations and stress changes utilizing GPS data and observed precipitation time series before an earthquake in Taiwan. Chang and Yeh (2016) studied solute transport in a saturated porous medium with variable hydraulic conductivity which deforms in response to mechanical loads. Pacheco and Fallico (2015) modelled the response of a confined aquifer to river stage variations and mechanical loading. Based on accurate measurements of in situ displacements, Murdoch et al. (2015) developed a viable technique to characterize average load changes that occur over vast areas of soil. Considering all these studies, it is well stablished that the pore pressure record for deep wells can give valuable information about moisture loading effects and groundwater dynamics.

The main purpose of this paper is to present a new MATLAB code that iterates on the total stress boundary condition of a COMSOL finite element (FEM) model to replicate the pore pressure time series that are measured in the field for shallow aquitards in which loading and water table effects are superposed. The optimization can be conducted with optional constraints on the water budget. An example based on pore pressure measurements for the Champlain clay deposit in Sainte-Marthe, Québec is presented (Shafaei et al. 2018). The conceptual approach that was applied in this paper is mainly based on the work of Biot (1941) and van der Kamp and Gale (1983).

2 SITE DESCRIPTION

The study site is located in the St. Lawrence River valley, in Sainte-Marthe, west of Montreal, Quebec. The clay layer is found from the surface to a depth of 16.0 m. The clay is fractured from the surface to a depth of 3.0 m and massive between depths of 3.0 to 14.0 m. Brownish, plastic clay can be found up to a depth of 7.5 m. Grey clay with a sensitivity of up to 200 can be found between depths of 7.5 and 14.0 m. From a depth of 14.0 m, the soil becomes progressively siltier with some sand and gravel. The bedrock is located 20.6 m below the surface.

This study site has three boreholes equipped with standpipe piezometers and vibrating wire piezometers (VWP). Water table fluctuations in the fractured clay and hydraulic head fluctuations in the bedrock are measured with pore pressure transducers in standpipe piezometers installed in the fractured clay layer and in the bedrock. VWP installed with the fully grouted method record the pore pressure changes at depths of 6.1 and 12.1 m in the clay layer. The hydraulic head simulation results that will be discussed in the following sections associated with the observed pressure heads obtained from the VWP at the depth of 12.1 m. More detailed descriptions of the study site were presented by Marefat et al. (2019) and Shafaei et al. (2018).

3 THEORETICAL BACKGROUND

The Biot-Darcy poroelasticity model can define the relationship between three-dimensional stress and strain along with seepage through a porous material. van der Kamp and Gale (1983) simplified the Biot theory for one-dimensional deformation and flow. They derived Eq. 1 describing the response of saturated porous media to uniform surface loading and transient flow. They assumed their domain to be horizontally constrained with negligible horizontal transient flow and strain.

$$\frac{\partial p}{\partial t} = \left(D \frac{\partial^2 p}{\partial z^2} + \gamma \frac{\partial \sigma}{\partial t}\right) \quad [1]$$

where p is the pore pressure, D is the hydraulic diffusivity, γ is the elastic pore pressure coefficient, and σ is the mechanical load.

4 CONCEPTUAL MODEL

Based on the van der Kamp and Gale (1983) theory, pore pressure changes in laterally constrained porous media can be obtained by measuring or estimating the stress change and by solving vertical transient flow with Eq. 1.

In order to use the van der Kamp and Gale (1983) 1D model, we need to consider specific assumptions. First of all, the flow regime in the soil should be transient and largely vertical. For this purpose, the fractured layer where the flow regime can be significantly affected by the presence of fractures was removed from our domain. As a result, our domain is a confined fully saturated clay layer.

The stress changes in the domain can be affected by tidal or barometric effects. By removing these effects, the stress term only reflects the stress changes due to moisture loading at the top boundary:

$$\sigma(0,t) = \rho_w g(P - ET - R) \quad [2]$$

where σ is the total stress, t is the time, ρ_w is the density of water, g is the gravity acceleration, and P, ET, and R are respectively cumulative precipitation, evapotranspiration, and runoff height. The vertical transient flow in the domain occurs in response to mechanical loading and pore pressures changes at the top and bottom boundaries. After estimating stress and pore pressure changes at the domain boundaries from the water table variation and the pore pressure record in the bedrock, pore pressure changes in the confined layer can be simulated utilizing the van der Kamp and Gale (1983) method.

5 FINITE ELEMENT MODEL

COMSOL Multiphysics implements the finite element method (COMSOL 2017). Its poroelasticity interface solves the Biot (1941) equations. A two-dimensional geometry was selected as this interface does not allow a one-

dimensional geometry. The top 3 m of fractured clay were excluded from the model as the hydraulic and mechanical processes in this layer are more complex (e.g. freeze/thaw, double porosity and matrix effect).

5.1 Boundary and initial conditions

Boundary conditions must be applied for the water conservation and static equilibrium equations. The total stress change is applied at the top boundary. It corresponds to Eq. 2. The hydraulic head condition at the top boundary corresponds to the water table elevation. It is estimated based on the groundwater level time series measured in the field for the simulation period. The bottom boundary of the domain is fixed (no displacement). The hydraulic head is set equal to the hydraulic head measured in the bedrock well. The lateral boundary conditions are chosen to replicate 1D flow and deformation.

The initial hydraulic head and displacement conditions were obtained from a steady-state simulation with the initial water table elevation and bedrock hydraulic head as boundary conditions and with a free displacement (zero total stress) condition at the top of the soil profile.

5.2 Material Properties

For each material, COMSOL's poroelasticity interface requires a Young's modulus, Poisson ratio, density, porosity and intrinsic permeability. Table 1 shows the geotechnical parameters for each layer. The intrinsic permeability of each layer was estimated using the Kozeny-Carman equation and based on water properties at 10°C (Chapuis and Aubertin 2003; Duhaime et al. 2013). A constant Young's modulus of 50 MPa was considered for all layers. It was estimated based on the barometric pressure response of the aquitard and triaxial tests conducted at ÉTS (Marefat et al. 2019). The barometric pressure response was calculated utilizing the van der Kamp and Gale (1983) theory.

Table 1. Geotechnical properties for the Sainte-Marthe study site

Depths (m)	Porosity (-)	Poisson ratio (-)	Dry density (kg/m^3)	Permeability (m^2)
3.0-7.5	0.60	0.3	1002	4.81×10^{-17}
7.5-11.0	0.65	0.3	1044	1.83×10^{-16}
11.0-14.0	0.60	0.3	1089	1.06×10^{-16}
14.0-15.3	0.47	0.3	1433	7.69×10^{-17}
15.3-20.6	0.40	0.3	1600	4.57×10^{-14}

5.3 Meteorological data and pore pressure records

The meteorological data including temperature, wind speed, relative humidity, precipitation as rain and snow were obtained from an experimental station located 2.2 km away from the study site in Sainte-Marthe. The evapotranspiration was estimated using the ETo Calculator software based on the FAO Penman-Monteith method (Allen et al. 1998; Raes 2012). The period of simulation begins from 2017/05/24 and ends on 2019/01/24. Daily time steps were used.

Pore pressure data were corrected for barometric effects using the multiple regression technique as described by Marefat et al. (2015). A Savitzky–Golay filter was applied on the corrected pore pressure for smoothing and removing the small fluctuations (Savitzky and Golay 1964).

6 MATLAB SCRIPT

The aim of the MATLAB script is to correct the model's stress input and, consequently, to modify the water budget on the study site (Eq. 2). The main logic behind these corrections is to find the optimum stress time series based on a comparison of simulated and recorded pore pressures in the aquitard. After removing barometric and tidal effects, assuming there is no change in mechanical loading except the variation in soil moisture, total stress fluctuations depend on the available volume of water in the fractured clay layer above our FEM domain.

Two methods were used in the MATLAB script for stress correction: the perfect stress method (PS) and the net water balance method (NWB).

6.1 Perfect stress method (PS)

With the PS method, the total stress value for each time step is simply selected so that the FEM pore pressure replicates the pore pressure that was measured in the field. For each daily time step, the total stress is calculated using the Newton–Raphson technique:

$$\sigma_{j+1}(i) = \sigma_j(i) + \left(Obs(i) - p_j(i)\right)\frac{\left(\sigma_j(i)-\sigma_{j-1}(i)\right)}{\left(p_j(i)-p_{j-1}(i)\right)} \quad [3]$$

where $\sigma(i)$ is the total stress on day i, $p(i)$ is the FEM pore pressure on day i, and Obs(i) is the measured pore pressure on day i. Indices j and j-1 refer to the previous iterations for the Newton-Raphson method, while j+1 refers to the current iteration. Since the pore pressure change is directly related to the stress change, it is always possible for the FEM pore pressure to match perfectly the field measurement. The main disadvantage of this method is that it does not verify if the net water balance is realistic.

6.2 Net water balance method (NWB)

The NWB method puts constraints on the stress time series based on the net water balance. Based on a simple water balance equation (Figs. 1 and 2), precipitation as snow and rain is added to moisture storage as snow cover (P_{sc}) or as near-surface groundwater (P_{rc}), while runoff and evapotranspiration are removed. The daily amount of precipitation and evapotranspiration is known, whereas daily runoff is unknown and must be calculated by the MATLAB script for each time step to replicate the pore pressure time series.

For day i, it is assumed that the water available for runoff (A_{wr}) is equal to the sum of precipitation as rain (P_r)

and snow (P_s, in equivalent water height), and the snow cover accumulated from the previous time step (P_{sc} also in equivalent water height):

$$A_{wr}(i) = P_r(i) + P_s(i) + P_{sc}(i) \quad [4]$$

The runoff for time step *i* is applied to the rain:

$$R_r(i) = R(i)\, P_r(i) \quad [5]$$

where R_r is the amount of rain leaving the system as runoff and R is a runoff coefficient between 0 and 1 that represents the fraction of A_{wr} that leaves the system as runoff. For snow, the runoff is assumed to be proportional to the sum of precipitation as snow and the snow cover:

$$R_s(i) = R(i)\,(P_s(i) + P_{sc}(i)) \quad [6]$$

The water available for evapotranspiration (A_{wet}) is not the same as A_{wr}. Evapotranspiration is assumed to impact the water stored as snow and rain at the beginning of the time step and the precipitation net of runoff:

$$A_{wet}(i) = \big(P_r(i) + P_s(i) + P_{sc}(i)\big)(1 - R(i)) + P_{rc}(i) \quad [7]$$

where $P_{rc}(i)$ corresponds to the amount of water stored as near-surface groundwater at the beginning of day *i*. The evapotranspiration of liquid water (ET_r) is proportional to the near-surface groundwater storage and rain, while the evapotranspiration of snow (ET_s) is proportional to the snow cover and precipitation as snow:

$$ET_r(i) = ET(i)\frac{P_r(i)(1-R(i))+P_{rc}(i)}{A_{wet}(i)} \quad [8]$$

$$ET_s(i) = ET(i)\frac{(P_s(i)+P_{sc}(i))(1-R(i))}{A_{wet}(i)} \quad [9]$$

where $ET(i)$ is the total evapotranspiration for day *i* calculated as described in section 5.3. The new near-surface groundwater storage and snow cover at the end of day *i* can be calculated using a simple water budget:

$$P_{rc}(i+1) = P_{rc}(i) + P_r(i) - ET_r(i) - R_r(i) \quad [10]$$

$$P_{sc}(i+1) = P_{sc}(i) + P_s(i) - ET_s(i) - R_s(i) \quad [11]$$

The total stress at the beginning of each day is calculated from the weight of a water column equivalent to the groundwater storage and snow cover:

$$\sigma(i) = \rho_w g\big(P_{rc}(i) + P_{sc}(i)\big) \quad [12]$$

The P_{sc}(i+1) value should either be zero or positive. Negative values should be replaced with zero and the water deficit should be transferred to P_{rc}(i+1). These simplifications and assumptions were made for making the model as simple as possible since the aim of this study is not to develop a hydrological model.

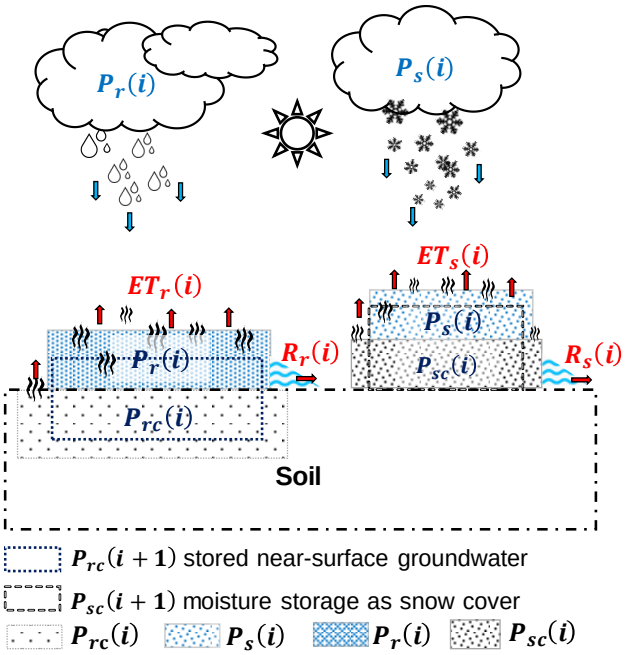

Figure 1. Components of the water balance equation.

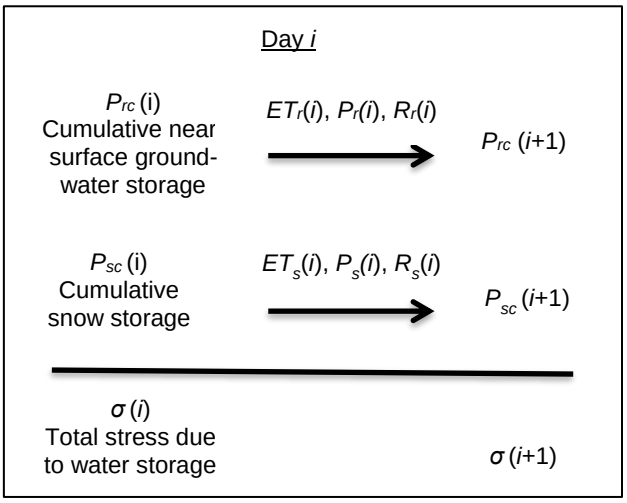

Figure 2. Schematic representation of the time-stepping scheme for day *i*.

The daily runoff ratio is the only unknown in Eqs. 4-12. Compared to the prefect stress method which finds the stress time series that best replicates the observed pore

pressure without any hydrological constraint, the NWB method is only allowed to change the daily *R* coefficient. This imposes a range on the $\sigma(i)$ values. The upper limit of this range occurs when we have no runoff. The lower limit is observed when the *R* coefficient takes its highest value. This maximum *R* can be specified by the user.

The $R(i)$ values were obtained using the Newton-Raphson method:

$$R_{j+1}(i) = R_j(i) + \left(Obs(i) - p_j(i)\right)\frac{\left(R_j(i) - R_{j-1}(i)\right)}{\left(p_j(i) - p_{j-1}(i)\right)} \quad [13]$$

where indices *j*-1, *j* and *j*+1 stand for the iteration numbers as in Eq. 3. Contrarily to the σ values with the PS method, the $R(i)$ values are bounded by 0 and 1, or some other upper value set by the user. The upper and lower $R(i)$ limits were used to estimate the slope of the relationship between *p* and *R* for the first iteration (i.e. $R_1(i) = 0$ and $R_2(i) = 1$).

The PS and NWB methods assume that the instantaneous pore pressure change can be used directly to estimate the moisture loading resulting in the best agreement between the simulated and measured pore pressure data. However, the stress change also has a smaller delayed impact on the pore pressure as the instantaneous pore pressure change dissipates. To verify this impact, stress increments of 1 kPa were applied sequentially for each time step. The impact on pore pressure for the following time steps was recorded. The unit stress increments were applied to a baseline scenario (BS) corresponding to $R(i) = 0$ for each time step. The results were used to define α values which correspond to the pore pressure change due to the unit stress increase compared to the baseline scenario:

$$\alpha\,(i,j) = p(i,j) - pref(j) \quad [13]$$

where $\alpha\,(i, j)$ shows the impact of a 1 kPa stress change applied on day *i* on the pore pressure measured on day *j*, $p(i,j)$ is the pore pressure on day j following a stress increase on day *i* and $pref(j)$ is the pore pressure on day j for the baseline scenario. The $\alpha(i,j)$ values define a square matrix whose size is defined by the number of days in the simulation (period):

$$\alpha = \begin{pmatrix} \alpha\,(1,1) & \alpha\,(1,2) & \dots & \alpha\,(1,period) \\ 0 & \alpha\,(2,2) & \dots & \alpha\,(2,period) \\ \dots & \dots & \dots & \dots \\ 0 & 0 & \dots & \alpha\,(period,period) \end{pmatrix} \quad [14]$$

As a stress change on day *i* does not influence the pore pressure on day $j < i$, the resulting matrix is an upper triangular matrix.

7 RESULTS AND DISCUSSION

Figure 3 compared the hydraulic head results for the PS and NWB methods with the experimental values. As defined by the method, the fit between the PS and experimental values is perfect. The difference between the experimental and NWB hydraulic head values increases in the second half of the simulated period. The agreement is generally good considering the added constraint for the water budget.

Several explanations can be given for the difference between the NWB and experimental hydraulic head values. First, it might be due to inaccuracies in meteorological data. For instance, the GMON device that measures the snow water equivalent may overestimate the snow precipitation by up to 30 % (Smith et al. 2017b). The difference might also be due to errors in the pore pressure measurements. Even with a perfect piezometer installation, measurement errors can be expected. The accuracy of the transducers measuring the water table height, the hydraulic head in the bedrock, and the pore pressure in the clay is approximately ±30 mm (Van Essen Instruments 2016; RST Instruments 2003). There could also be some significant differences between the real evapotranspiration and the Penman-Monteith estimation. Evapotranspiration from tree canopies, especially during dry periods, can result in soil moisture losses (Smith et al. 2017a). This factor was not considered in the water budget.

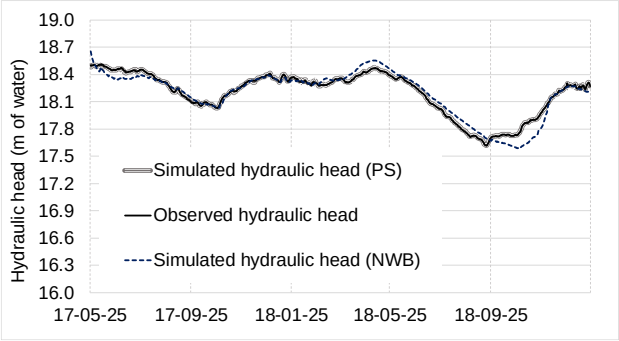

Figure 3. Comparison of observed and simulated hydraulic head time series for the PS and NWB methods (depth of 12.1 m).

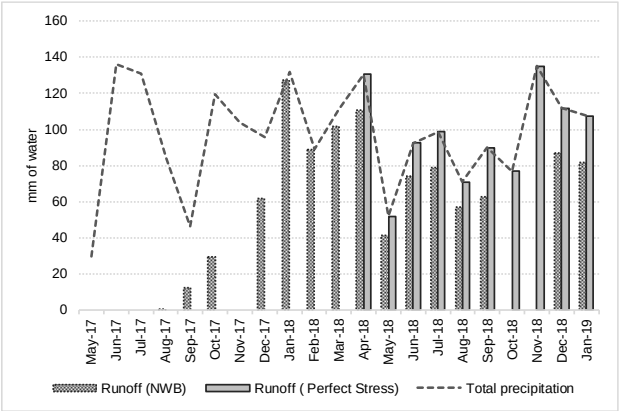

Figure 4. Comparison of runoff values from perfect stress method and weighted method.

Figure 4 shows the monthly runoff values that were calculated with the NWB and PS methods. The runoff ratios for the PS method are below 0 in the first half of the period and greater than 1 in the second half. These unrealistic ratios can probably be explained in part by errors in the other terms of the water balance and by the influence of the initial condition of the numerical model. For example, an increase in evapotranspiration during summer that is not captured by the Penman-Monteith method could explain runoff ratios larger than 1 for the PS method and hydraulic head values that are higher than the field measurements for the NWB method. The NWB and PS methods also do not consider the delayed impact of stress changes on pore pressures which will discussed later with the α matrix.

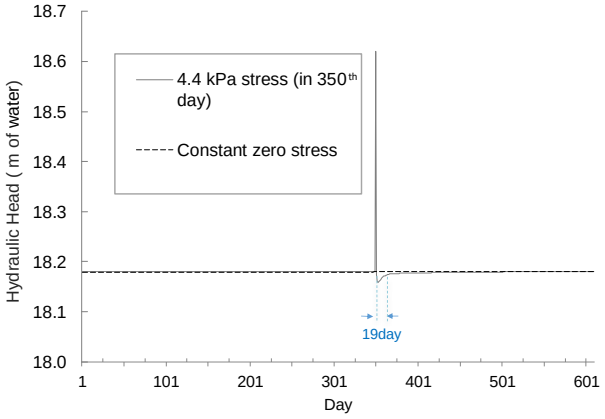

Figure 5. Comparison of hydraulic head values with constant zero stress and after applying a 4.4 kPa stress increase on the 350th day.

The cumulative nature of stress changes can be another source of error as an error in one time step will influence the following time steps. The first half of the period is also influenced by the model initial conditions. At the beginning of the period, the piezometer record is still influenced by the transient effects of hydrological changes that occurred prior to the simulation period.

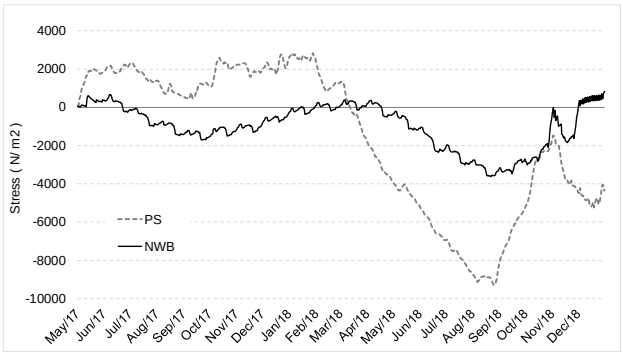

Figure 6. Comparison of stress values obtained with the NWB and PS methods.

Assuming the amplitude of the fluctuations prior to May 2017 was the same as during the simulation period, the difference between maximum or minimum and average pore pressures will be a water column of 0.45 m or 4.4 kPa. A simulation can show that the pore pressure change induced by this excess pore pressure can last about 19 days (Fig. 5). This implies that the results obtained for the first 19 days of the simulation period should be considered unreliable.

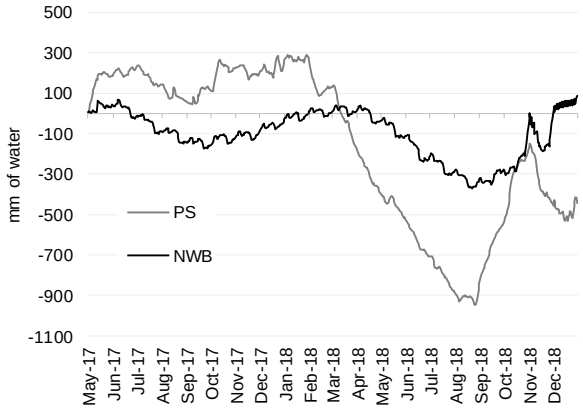

Figure 7. Change in the height of water stored as snow and shallow groundwater with the PS and NWB methods.

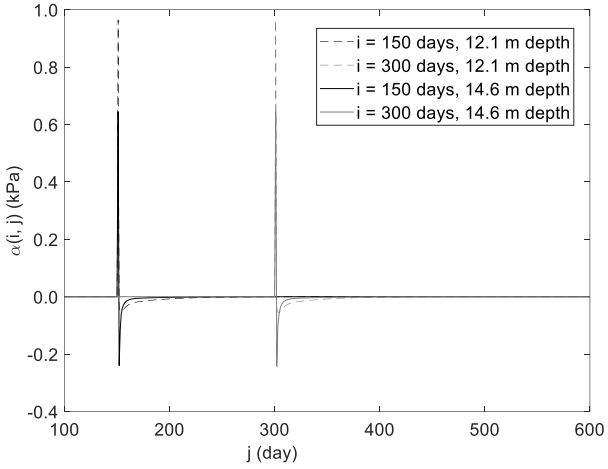

Figure 8. Examples of lines from the α matrices for two depths of 12.1 and 14.6 m in the clay layer.

Figures 6 and 7 show the stress boundary conditions for the NWB and PS methods expressed respectively in Pa and mm of water. The PS method resulted in very high runoff ratios during the summer months of 2018. Figures 6 and 7 imply an annual water storage cycle with amplitudes of 300 and 1200 mm for the NWB and PS methods, respectively. The change in water storage for the PS method appears large considering the total thickness of the soil profile on the Sainte-Marthe site (20.6 m).

Figure 8 shows selected lines (constant *i* values) for the α matrices that were obtained for depths of 12.1 and

14.6 m from the soil surface. The $\alpha(i, j)$ values correspond to the pore pressure change on day j resulting from a stress increase of 1 kPa on day i. The first day following the stress increase ($j = i$) shows a positive α value related to the elastic pore pressure coefficient (γ in Eq. 1) and to the distance from the nearest constant head boundary (fractured clay at the top and coarser grained layer at the bottom). The following days show a decrease in stress compared to the baseline simulation. This delayed decrease is due to the pore pressure change occurring near the constant-head boundaries: the stress increase is partially dissipated as it is applied. This leads to a net pore pressure decrease near the constant head boundaries when the 1 kPa stress is removed.

Both the PS and NWB methods only consider the instant pore pressure change due to moisture loading ($\alpha(i,j)$ for $i = j$). Although the delayed pore pressure changes are less significant, they could also be considered for the choice of the optimal moisture loading. This delayed effect might be another reason behind the inaccuracies of the NWB simulation. Developing a method that takes into account the effect throughout the simulation period can be an interesting subject for future work.

8 CONCLUSION

This study proposed a new technique for calculating the total stress boundary condition at the top of a soil column to replicate the pore pressure record obtained in the field. Two methods were presented. The PS method does not consider the water balance and finds a total stress boundary condition that replicates the pore pressure record perfectly. The NWB method puts constraints on the total stress boundary condition based on a simple water balance equation. The two methods were compared using data from the Sainte-Marthe study site. The results demonstrate the ability of the model and MATLAB interface to obtain the net water balance components.

There are still some inaccuracies that should be improved in measurements or assessment of meteorological data and pore pressure record. For instance, a methodology can be developed to take into consideration the delayed impact of stress changes. Accurate measurements of evapotranspiration would also result in a more accurate water balance and improvements in the estimation of stress changes. Extending the observation period could also result in a better optimization and interpretation of pore pressure changes.

9 ACKNOWLEDGMENTS

The authors gratefully acknowledge the support of NSERC for this research project.

10 REFERENCES

Allen, R., Pereira, L., Raes, D., and Smith, M. 1998. Crop evapotranspiration - Guidelines for computing crop water requirements, *FAO Irrigation and drainage paper 56*, FAO, Rome.

Anochikwa, C.I., van der Kamp, G., and Barbour, S.L. 2012. Interpreting pore-water pressure changes induced by water table fluctuations and mechanical loading due to soil moisture changes, *Canadian Geotechnical Journal*, 49: 357–366.

Barr, A.G., van der Kamp, G., Schmidt, R. and Black, T.A.,. 2000. Monitoring the moisture balance of a boreal aspen forest using a deep groundwater piezometer, *Agricultural and Forest Meteorology*, 102(1): 13–24.

Biot, M.A. 1941. General theory of three-dimensional consolidation, *Journal of Applied Physics*, 12(2): 155-164.

Chang, C.-M., and Yeh, H.-D. 2016. Investigation of flow and solute transport at the field scale through heterogeneous deformable porous media, *Journal of Hydrology*, 540: 142–147.

Chen, C.H., Tang, C.C., and Cheng, K.C. 2015. Groundwater-strain coupling before the 1999 Mw 7.6 Taiwan Chi-Chi earthquake, *Journal of Hydrology*, 524: 378–384

COMSOL. 2017. *COMSOL Multiphysics 5.3 Reference Manual*. COMSOL AB, Stockholm.

Duhaime, F.F., Benabdallah, E.M., and Chapuis, R.P. 2013. The Lachenaie clay deposit : some geochemical and geotechnical properties in relation to the salt-leaching process, *Canadian Geotechnical Journal*, 325: 311–325.

Hayashi, M. and Farrow, C.R. 2014. Watershed-scale response of groundwater recharge to inter-annual and inter-decadal variability in precipitation (Alberta, Canada). *Hydrogeology Journal*, 22(8): 1825–1839.

Marefat, V., Duhaime, F., and Chapuis, R.P. 2015. Pore pressure response to barometric pressure change in Champlain clay: Prediction of the clay elastic properties, *Engineering Geology*, 198: 16–29.

Marefat, V., Duhaime, F., Chapuis, R. P., and Le Borgne, V. 2019. Performance of fully grouted piezometers under transient flow conditions: field study and numerical results, *Geotechnical Testing Journal*, 42(2): 433–456.

Murdoch, L.C., Freeman, C.E., Germanovich, L.N., Thrash, C., and Dewolf, S. 2015. Using in situ vertical displacements to characterize changes in moisture load, *Water Resources Research*, 51(8): 5998–6016.

Pacheco, F.A.L., and Fallico, C. 2015. Hydraulic head response of a confined aquifer influenced by river stage fluctuations and mechanical loading, *Journal of Hydrology*, 531: 716–727.

Raes, D. 2012. *The ETo Calculator*. Reference Manual Version 3.2, FAO, Rome.

RST Instruments. 2003. *Vibrating Wire Piezometer*. RST Instruments LTD, Maple Ridge.

Savitzky, A., and Golay, M.J.E. 1964. Smoothing and Differentiation of Data by Simplified Least Squares Procedures. *Analytical Chemistry*, 36(8): 1627–1639.

Shafaei, A., Duhaime, F., and Marefat, V. 2018. Numerical simulation of pore pressure changes in Champlain clays - Sainte-Marthe study case, 71st Canadian Geotechnical Conference, Edmonton, AB

Smith, C.D., van der Kamp, G., Arnold, L., and Schmidt, R. 2017a. Measuring precipitation with a geolysimeter,

Hydrology and Earth System Sciences, 21(10): 5263–5272.

Smith, C.D., Kontu, A., Laffin, R., and Pomeroy, J.W. 2017b. An assessment of two automated snow water equivalent instruments during the WMO Solid Precipitation Intercomparison Experiment, *Cryosphere*, 11(1): 101–116.

Van Essen Instruments. 2016. *Product Manual-Diver*. Van Essen Instruments, Delft.

van der Kamp, G., and Gale, J.E. 1983. Theory of earth tide and barometric effects in porous formations with compressible grains, *Water Resources Research*, 19(2): 538–544.

van der Kamp, G., and Maathuis, H. 1991. Annual fluctuations of groundwater levels as a result of loading by surface moisture, *Journal of Hydrology*, 127(1–4): 137–152.

van der Kamp, G., and Schmidt, R. 2017. Review: Moisture loading—the hidden information in groundwater observation well records, *Hydrogeology Journal*, 25(8): 2225–2233.